arXiv:1403.4840v1 [physics.ao-ph] 19 Mar 2014

Bursts in intermittent aeolian saltation

M. V. Carneiro[1], K. R. Rasmussen[2], and H. J. Herrmann[1,3]
[1] *Institut für Baustoffe, ETH-Hönggerberg, Schafmattstrasse 6, 8093 Zürich, Switzerland*
[2] *Department of Geoscience, Aarhus University, Hoegh Guldbergsgade 2, 8000 Aarhus C, Denmark and*
[3] *Departamento de Física, Universidade Federal do Ceará, 60451-970 Fortaleza, Ceará, Brazil*
(Dated: March 20, 2014)

Close to the onset of Aeolian particle transport through saltation we find in wind tunnel experiments a regime of intermittent flux characterized by bursts of activity. Scaling laws are observed in the time delay between each burst and in the measurements of the wind fluctuations at the critical Shields number θ_c. The time delay between each burst decreases on average with the increase of the Shields number until saltation becomes non-intermittent and the sand flux becomes continuous. A numerical model for saltation including the wind-entrainment from the turbulent fluctuations can reproduce these observations and gives insight about their origin. We present here also for the first time measurements showing that with feeding it becomes possible to sustain intermittent flux even below the threshold θ_c for natural saltation initiation.

Sporadic bursts of sand and dry soil are common wind erosion events. Through them, a granular surface can be slowly eroded even at rather low wind strength, contributing to long-term changes in the landscape [1]. Bursts occur when the wind velocity fluctuates around the threshold controlling the initiation of sand movement. Despite being quite common, little is known about this intermittent saltation mechanism.

In the laboratory, Bagnold observed that when the wind velocity above a quiescent sand surface increases above a certain limit some grains are for a short moment lifted into the air flow and gain momentum. When subsequently colliding with the bed and ejecting other sand grains saltation accelerates to an equilibrium value through a cascading reaction. The shear velocity of the wind flow at the minimum threshold for Aeolian particle entrainment Bagnold named the static (fluid) threshold u_t [2, 3]. Bagnold also observed that once started, saltation will cease at a somewhat lower shear velocity due to momentum transfer from the impacting grains. This he named the dynamic (impact) threshold u_D. The ratio between the dynamic and the statistic threshold is 0.80 [2].

In the field, Rasmussen and Sørensen observed saltation to start and evolve temporarily below the fluid threshold [4]. Likewise, Jackson observed that saltation has inertial properties and may continue after the shear velocity drops below the fluid threshold [5]. Turbulent fluctuations of the wind velocity around the threshold produce coherent structures such as patchiness in saltation and sand streamers [6, 7]. The burst effects of turbulence were first identified in sediment transport in water [8, 9]. In aeolian saltation, Stout defined an intermittency function and found that bursts of saltation were approximately normally distributed with respect to the relative wind strenght [1]. Schönfeldt studied intermittent saltation considering the fluid and dynamic thresholds [10]. All studies mentioned here were performed in the field, i.e. not under reproducible or fully controlled conditions. Based on laboratory studies and numerical simulations we will present here the first systematic investigation of intermittent saltation allowing us to explore quantitatively an astonishingly rich phenomenon.

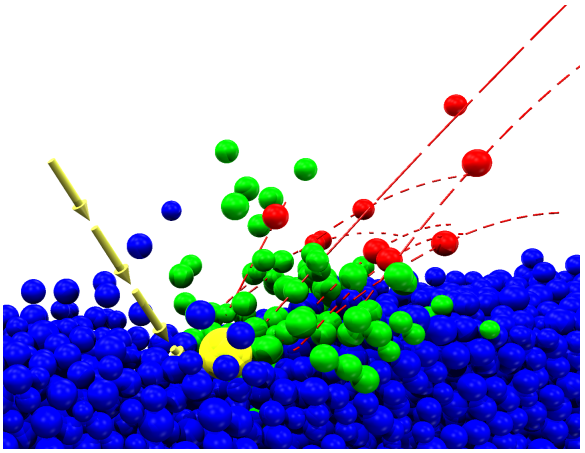

FIG. 1. (color online). The numerical simulation of a high energy particle splash ejecting other particles in the saltation process. The fastest ejected particles are coloured in red. Low energy impacts might eject no particles ending saltation.

Here, we report bursts in intermittent saltation not only experimentally observed in a wind tunnel but also numerically reproduced using a stochastic process to model the temporal fluctuations in a turbulent channel flow. The discrete element model reproduces the rich variety of particle splashes that explain the sand bursts. Numerical results match the transport of sand observed in the wind tunnel. For instance, Fig 1. shows the numerical simulation of a high energy particle splash ejecting other particles in the saltation process. Splashes might also not have the necessary energy to eject any particles [11]. The interplay between those weak splashes and the turburlent entrainment from the wind constitutes the mechanism behind the statistics of sand bursts.

At Aarhus university, we used a wind tunnel illustrated in Fig. 2. The wind tunnel is 15 m long with 5 m of working section in the downstream end. Wind flow is created by a fan in the downwind end (suction) and the fan set-

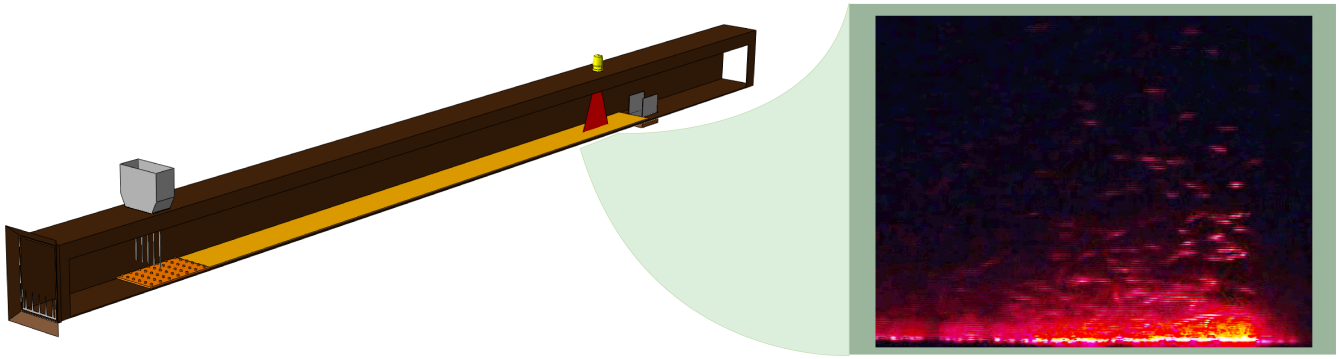

FIG. 2. (color online). (a) Experimental set-up of the wind tunnel. (b) A snapshot of the sand transport in the wind tunnel.

ting can be adjusted between 0 and 50 Hz with a resolution of 0.1 Hz. The relation of the wind shear velocity as function of the fan setting is shown in the Supplemental Material [12]. The rectangular cross section is 0.60 m wide and 0.90 m high. A set of turbulence spires at the entry and a 4 m long array of roughness blocks downwind of the spires have been designed to produce a boundary layer which has approximatelly the same characteristics as that forming over an infinitely long sand bed near the fluid threshold [13]. Downwind of the array, the bottom of the tunnel is covered by a 15 mm thick bed of presieved sand samples of diameter $D_{mean} = 180\mu$m. Feeding is appropriate for studying saltation when the shear stress is above the dynamic threshold, and normally sand is fed into the tunnel via 5 tubes that will distribute it fairly evenly across the bed. The feeding rate is approximately the same as that by which sand is transported downstream the tunnel. This will simulate an infinite upwind fetch and also prevent the upwind end of the bed to be depleted of sand.

Contrary to this, feeding must be avoided when studying the grain pick-up as a result of aerodynamics lift. However under this condition, the transport rate is low so that the 15 mm thick bed still allows fairly long experiments to be made before depletion occurs. A small container at the end of the working section collects the transported sand from which we obtain the average flux.

Saltation is recorded on a standard video camera (2 megapixels) outside the tunnel. This focuses on the central part of the tunnel where saltating particles are illuminated when they cross a vertical laser sheet. Color frames are extracted from the videos (see Fig. 2) and converted to grayscale and then into binary black and white images using a low pixel threshold thus trying to keep the noise level low. Some particles may be lost during this selection. The intensity of the saltation flux is then determined from the number of white pixels. We observe the bursts in saltation through the increase of white pixels in the images. We define the start and end of a burst to occur when the change in the number of white pixels from one frame to the next is more than 70.

Initially the duration of experiments varied from 2-3 minutes (short-runs), but this produced very poor statistics. Therefore two series of new experiments were made where data were taken over three consecutive periods of 20 minutes (long-runs). The environmental conditions are described in the Supplemental Material [12].

In the numerical simulations, a poly-disperse 3D packing of hard spheres of gaussian distributed diameters with $D_{mean} = 2 \times 10^{-4}$ m, size dispersion $\sigma_D = 0.15 D_{mean}$, and density $\rho_s = 2650$ kg/m^3, in a three-dimensional wind channel of dimension $(700 \times 50 \times 7.5) D_{mean}^3$ is subjected to a gravitational field in vertical direction (y-direction) and a logarithmic wind velocity profile $u(y)$ imposed in horizontal direction (x-direction),

$$u(y) = \frac{u_*}{\kappa} \ln \frac{y - h_0}{y_0}. \tag{1}$$

In Eq. (1), $y_0 = D_{mean}/30$ is the roughness of the bed, h_0 the bed height, $\kappa = 0.4$ the von Kármán constant, and u_* the wind shear velocity. The air density is $\rho_a = 1.174$ kg/m^3. The dynamic integration of the wind profile explained in the Supplemental Material considers the momentum exchange between the wind and the grains [12]. We express the wind velocity through the dimensionless Shields number, defined as

$$\theta = \frac{u_*^2}{(\rho_s/\rho_a - 1) g D_{mean}}. \tag{2}$$

The wind drag is the only external force applied to the particles along the x-direction,

$$\mathbf{F}_d = -\frac{\pi D^2}{8} \rho_a C_d v_r \mathbf{v_r}, \tag{3}$$

where $\mathbf{v_r} = \mathbf{v} - \mathbf{u}$ is the velocity difference between particle and wind, with $v_r = |\mathbf{v_r}|$, and C_d is the drag coefficient [14].

The turbulent flow velocity $\mathbf{u}$ splits into the mean stream velocity $\mathbf{u}(y)$ and a stochastic part $\mathbf{u}_t$:

$$\mathbf{u} = \mathbf{u}(y) + \mathbf{u}_t. \tag{4}$$

Reynolds [15] formulated a system of SDEs that reproduces the highly non-Gaussian behavior of the Lagrangian acceleration distribution of fluid particles in

fully developed turbulence. Every particle is attached to a tracer that generates random perturbations, for which the probability distribution width is controlled by the dissipation rate $\langle\varepsilon\rangle$. Details of this turbulence model are given in the Supplemental Material [12].

The trajectories of the particles are obtained using velocity Verlet and a spring dashpot with the restitution coefficient $e = 0.6$ [16]. Further information in the Supplemental Material describes the contacts between particles [12]. We use periodic boundary conditions in the direction of the wind to mimic an infinite system. We place a reflective upper boundary sufficiently high to avoid any particle colliding against it and the lower boundary at $y = 0$, representing the deep ground, is strongly dissipative with a fixed restitution coefficient of $e_w = 0.5$. We consider a bed of 12 particle layers to suppress the reflection of shock waves on the lower boundary due to the finite depth [17–19].

To compare the numerical results to the experiments, we determine the mass-flux defined as,

$$q = \rho_s C A \langle v_x \rangle, \tag{5}$$

where $A = (1000 \times 7.5) D_{mean}^2$ is the section area of the channel, C is the volume fraction of the particles, $\langle v_x \rangle$ the average velocity of the particles in the horizontal direction.

The intermittent saltation starts at the discontinuous threshold and the sand transport occurs in bursts. Without the sand feeding, the experiments in the wind tunnel for $\theta_c < 0.0072$ produced no grain at the end of the wind tunnel. The sand transport shoots up very steeply at $\theta_c \approx 0.0072 \pm 2 \times 10^{-5}$. Figure 3a shows the transported sand (red circles) collected at the container at the downwind end during the long runs. The value of the critical Shields number θ_c depends on the humidity and therefore it varies according to the weather conditions under which the experiments are performed [20]. Therefore, we normalize the wind shear velocities with θ_c. The dashed lines at θ_c show that the results are consistent with either a continuous or a discontinuous transition as reported in Ref [21]. Within the error bars, saltation activity is very rare and the sand flux is virtually zero for $\theta/\theta_c = 0.93$ as shown in the flux series on Fig 3b. The gradual increase of θ/θ_c shows the build up of the continuous flux (Fig. 3d) going through the intermittent state (Fig. 3c). As the wind velocity increases, the average burst size increases until the sand flux becomes continuous. Therefore, the interval of intermittent saltation is $1 < \theta/\theta_c \lesssim 1.25$. The numerical data from simulations (black squares) are discussed at the end of the manuscript.

Figure 4a shows the time series of the sand transport in the experiments at θ_c. An example of a sand burst from the video observations is highlighted in red. The burst size in yellow and the time delay between bursts in blue display scaling laws. Figure 4b shows that the burst size distribution follows a power law with exponent -0.7.

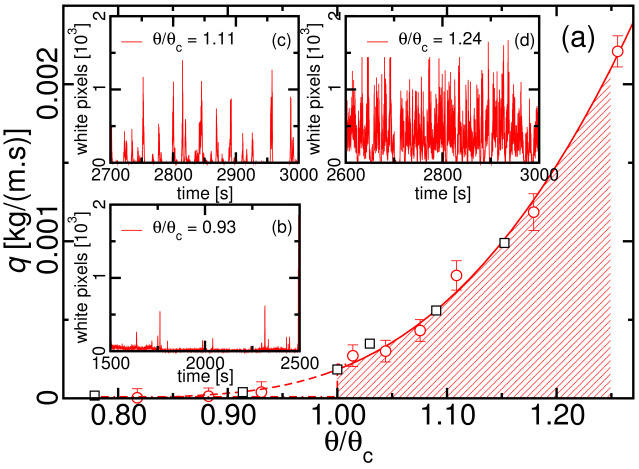

FIG. 3. (color online). The sand transport rate in the long experiments. In (a), the transport rate obtained from the sand collected in the experiments (red circles) compared with results from the numerical simulations (black squares). In (b), (c) and (d) show the time series obtained from the video analysis. Winds with Shield number below the critical Shields number tranport nearly no sand, as shown in (b). Saltation is intermittent for Shields numbers slightly above the critical Shields number $1 < \theta/\theta_c \lesssim 1.25$ and non-intermittent for $\theta/\theta_c > 1.25$, as shown in (c) and (d) respectively.

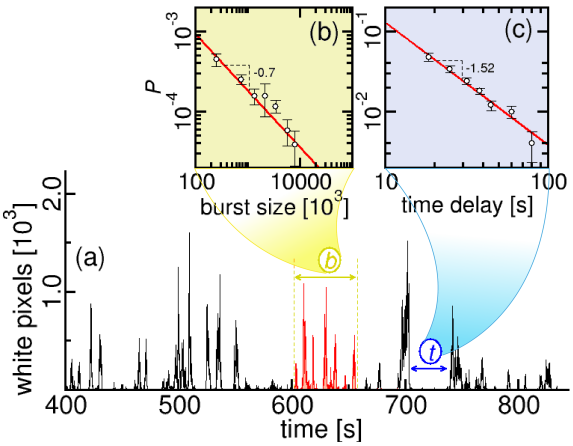

FIG. 4. (color online). (a) The time series of intermittent saltation at θ_c. In (b), the burst size is obtained from the integration of the events within the yellow dashed lines in (a). The burst size distribution is fitted by a power law with an exponent -0.7. In (c), the time delays between the sand bursts illustrated by the blue arrow also follow a power law distribution with exponent -1.52.

The time delay (or waiting time) between bursts has also a power law distribution with exponent -1.5, as shown in Fig. 4c. Scaling laws with comparable exponents can be also found in other complex systems with bursting activity, such as neuronal avalanches in rat cortex [22]. At $\theta/\theta_c = 1.24$, the short and few intervals between bursts require much longer runs for getting good statistics. The

high frequencies of the distribution are bounded by the noise stemming from the video camera. The low frequencies are bounded by the finite size of the wind tunnel which limits the formation of large low frequency eddies in the turbulent structure. Consequently, the probability distributions are restricted to a few orders of magnitude. The bursting activity was not prominent enough to observe a power law for $\theta < \theta_c$. Similar power laws fitted reasonably the time delays of the bursting activity for $\theta/\theta_c < 1.1$. However, for $\theta/\theta_c > 1.1$, it is more dificult to obtain a clear distribution for the reducing time delays.

Whether a burst is generated locally from strong gusts at the area nearby or from the gradual development of the saltation initiated far upstream and propagating downstream cannot be determined unless we measure the velocity at a series of upstream observation points. Figure 5 shows the wind velocity at the observation point for a run at the critical Shield's number θ_c. In red we show the periods where the wind velocity was larger than the average wind speed, i.e., the speed corresponding to θ_c. The time delay/waiting time between wind fluctuations above the average velocity also follows a power law of exponent -1.6, as shown in Fig. 5b. Similarities in the probability distributions strongly connect the occurence of the bursts to fluctuations in the wind speed.

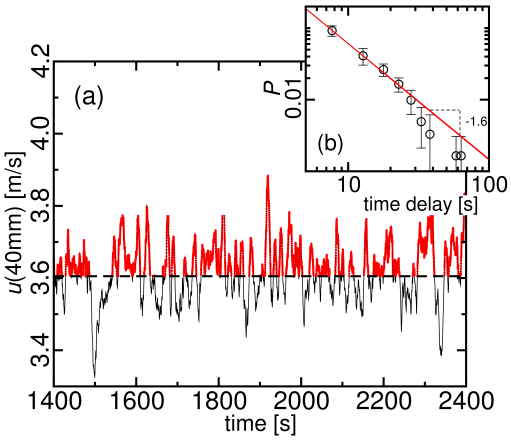

FIG. 5. (color online). In (a), the wind fluctuations measured at 40 mm above the sand bed at θ_c. In (b), the probability distribution of the time delays between the wind fluctuations in red is fitted by a power law with exponent -1.6.

The bursting of saltation can be turned on and off within a very short shear velocity interval. Figure 6a shows that bursts disappear and intermittent saltation stops, when the wind shear velocity of a 10 min run is switched down at t = 5 min from $\theta/\theta_c = 1$ to $\theta/\theta_c = 0.94$. Alternatively, the bursting appears immediately after the wind shear velocity is switched up again from $\theta/\theta_c = 0.94$ to $\theta/\theta_c = 1$.

Figure 7 shows two different experiments, with (red squares) and without feeding (black circles), that verified the hysteresis in saltation around the critical Shields number. The red curve shows the mass transport in the

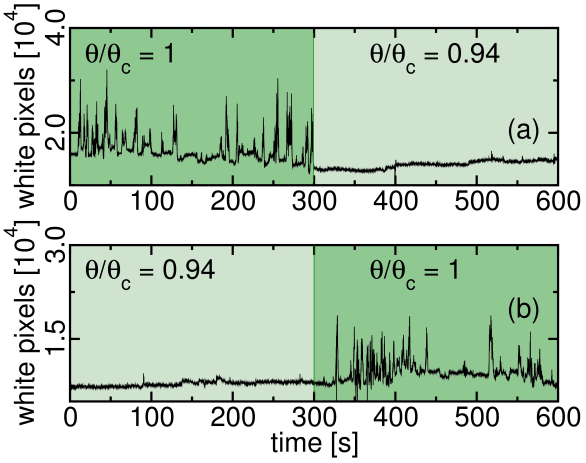

FIG. 6. (color online). In (a), the bursting activity at θ_c immediately ceases when the Shields number is decreased to $\theta/\theta_c = 0.94$. In (b), bursts start a few seconds after the Shields number increases from $\theta/\theta_c = 0.94$ to the critical Shields number θ_c.

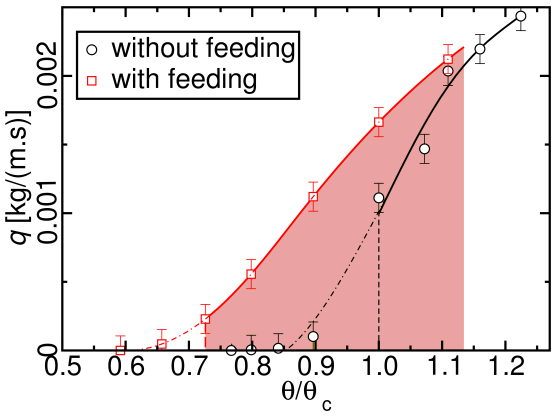

FIG. 7. (color online). The short experiments with (red squares) and without feeding (black circles) show the hysteresis zone (red area) between $\theta/\theta_c = 1.12$ and the dynamic threshold at $\theta/\theta_c = 0.73$.

experiments using grain feeding. With feeding it becomes possible to sustain intermittent flux even below the threshold θ_c for natural saltation initiation. The input of particles through feeding at the upwind end of the tunnel triggers saltation by adding momentum to the system and thus sustains transport as long as the wind shear velocity is above the dynamic threshold. Thus sand flux can occur for Shields numbers that did not display any transport without feeding. The feeding significantly shifts the critical Shields number to $\theta/\theta_c = 0.73$. The dashed lines at θ_c show that the results are consistent with either a continuous or a discontinuous transition for both experiments with and without feeding. The area in red shows the hysteresis zone that ends at $\theta/\theta_c = 1.12$ where the transported sand is the same for both experiments within the error bars. The contribution of the feeding to the sand transport decreases as $\theta/\theta_c \to 1.12$. We

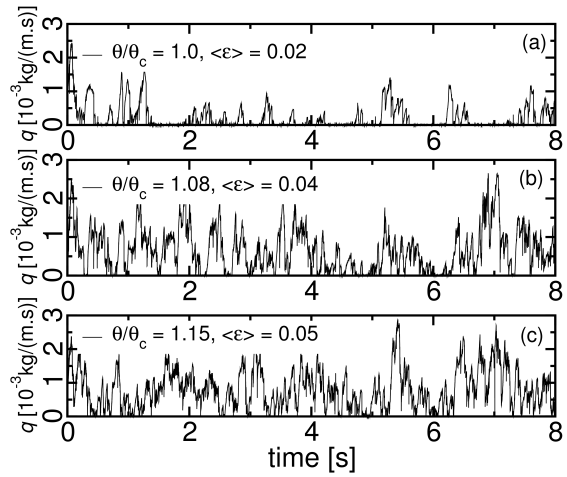

FIG. 8. Numerical simulation of intermittent saltation for different values of $\langle\varepsilon\rangle$. A completely settled particle bed, perturbations lift particles from the bed surface increasingly with $\langle\varepsilon\rangle$ and trigger saltation.

note that the ratio between critical Shields number with and without feeding is around 0.70 (or $u_D/u_t = 0.84$).

Random turbulent perturbations mimick the wind pick of sand grains by the wind eddies in the numerical simulation of saltation and reproduces the sand bursts observed in the experiments. The width of the distribution defined by $\langle\varepsilon\rangle$ controls the rate of particle lift. Wider distributions produce stronger turbulent accelerations. By adjusting $\langle\varepsilon\rangle$, the saturated flux of the numerical simulations (black squares) is found to match the sand flux observed in the experiments and reproduce the range of intermittent saltation, as shown by Fig. 3. Figure 8a shows the bursting activity at the sand flux at θ_c and $\langle\varepsilon\rangle = 0.02$ at the numerical simulations. From a completely settled particle bed, winds with dissipation rate $0.001 < \langle\varepsilon\rangle < 0.006$ detach particles from the bed surface starting saltation. However, the particle splash might eject no particles at low wind shear velocities and very inelastic particle collisions. If other particles are neither ejected nor lifted by the stochastic force meanwhile, saltation stops. Saltation restarts if any other saltating particle is detached from the particle bed by the stochastic turbulent forces. Increasing $\langle\varepsilon\rangle$, the lift rate increases and the time delay between sand burst decreases until sand flux becomes continuous. Winds with dissipation rates $\langle\varepsilon\rangle < 0.001$ entrain no particles, and $\langle\varepsilon\rangle > 0.006$ produces a continuous flux by entraining many particles.

We can not expect a perfect match between our findings in the wind tunnel and Nature. Experiments do not reproduce the low frequency of big eddies normally observed in the field. The wind shear velocity is a mean quantity which does not account the large temporal fluctuations of the wind. The bursting of saltation, and consequently the transported sand, has a nonlinear dependence on wind fluctuations. Therefore, the same wind shear velocity could have different rates of mass transport in the field and in the wind tunnel.

In summary, the turbulent gusts create intermittent saltation through bursting, which could be simulated numerically for the first time in a DEM simulation. Intermittent saltation occurs at Shields numbers between $1 < \theta/\theta_c \lesssim 1.25$. For $\theta/\theta_c \gtrsim 1.25$ saltation is non-intermittent and the saturated flux is continuous. Both wind measurements and video analysis displayed scaling laws and connect the burst initiation with the wind fluctuation above the wind threshold for the sand transport. In Nature, Shields numbers around the fluid threshold are very common, therefore bursting should be given more attention despite the major experimental difficulties. Future numerical work should improve the turbulent model including spatial correlations while future experiments could investigate the spatial coherence in the bursting process.

We thank Nuno Araújo, Eric Parteli, Thomas Pähtz and Jens Jacob Iversen for discussions and acknowledge the Brazilian Council for for Scientific and Technological Development (CNPq) and the European Research Council (ERC) Advanced Grant 319968-FlowCCS for financial support.

[1] J. Stout and T. M. Zobeck, Sedimentology **44**, 959 (1997)
[2] R. A. Bagnold, Proc. R. Soc. London A **157**, 594 (1936)
[3] R. A. Bagnold, *The Physics of Blown Sand and Desert Dunes* (Dover Publications, 2012) p. 265
[4] K. R. Rasmussen and M. Sørensen, Earth Surf. Process. Landforms **24**, 413 (199)
[5] D. Jackson, Sedimentary Geology **106**, 193 (1996)
[6] A. C. W. Baas and D. J. Sherman, J. Geophys. Res. **110** (2005)
[7] Y. Shao, *Physics and Modelling of Wind Erosion* (Kluwer Acad., Dordrecht, Amsterdan, 2008)
[8] A. D. Heathershaw, Nature **248**, 394 (1974)
[9] A. D. Heathershaw and P. Thorne, Nature **316**, 339 (1985)
[10] H. J. Schönfeldt, Meteorologische Zeitschrift **13**, 437 (2004)
[11] M. V. Carneiro, N. A. M. Araújo, T. Pähtz, and H. J. Herrmann, Phys. Rev. Lett. **111**, 058001 (2013)
[12] See Supplemental Material at, ...
[13] J. D. Iversen and K. R. Rasmussen, Sedimentology **46**, 723 (1999)
[14] N. S. Cheng, J. Hydraul. Eng. **123**, 149 (1997)
[15] A. M. Reynolds, Phys. Rev. Lett. **91**, 084503 (2003)
[16] M. Griebel, S. Knapek, and G. Zumbusch, *Numerical Simulation in Molecular Dynamics: Numerics, Algorithms, Parallelization, Applications* (Springer, New York, 2007)
[17] F. Rioual, A. Valance, and D. Bideau, Phys. Rev. E **62**, 2450 (Aug 2000)
[18] F. Rioual, Ph.D. thesis, University of Rennes 1 (2002)

[19] F. Rioual, A. Valance, and D. Bideau, Europhys. Lett. **61**, 194 (2003)
[20] McKenna-Neuman, Bound.-Layer Meteor. **108**, 61 (2003)
[21] M. V. Carneiro, T. Pähtz, and H. J. Herrmann, Phys. Rev. Lett. **107**, 098001 (2011)
[22] F. Lombardi, H. J. Herrmann, C. Perrone-Capano, D. Plenz, and L. de Arcangelis, Phys. Rev. Lett. **108**, 228703 (2012)